Inorganic Chemistry

Article

pubs.acs.org/IC

Unexpected Roles of Interstitially Doped Lithium in Blue and Green Light Emitting $Y_2O_3:Bi^{3+}$: A Combined Experimental and Computational Study

Sovann Khan,[†,‡,⊥] Heechae Choi,[§,⊥] Seung Yong Lee,[†,‡] Kwang-Ryeol Lee,[†,§] Odireleng Martin Ntwaeaborwa,[∥] Seungchul Kim,[†,§] and So-Hye Cho*[,†,‡]

[†]Department of Nanomaterial Science and Engineering, Korea University of Science and Technology, 217 Gajeong-ro Yuseong-gu, Daejon 04763, Republic of Korea

[‡]Materials Architecturing Research Center, Korea Institute of Science and Technology, Hwarangno 14-gil 5, Seongbuk-gu, Seoul 02792, Republic of Korea

[§]Computational Science Research Center, Korea Institute of Science and Technology, Hwarangno 14-gil 5, Seongbuk-gu, Seoul 02792, Republic of Korea

[∥]School of Physics, University of the Witwatersrand, Private Bag X3, Wits 2050, South Africa

Supporting Information

ABSTRACT: To enhance the photoluminescence of lanthanide oxide, a clear understanding of its defect chemistry is necessary. In particular, when yttrium oxide, a widely used phosphor, undergoes doping, several of its atomic structures may be coupled with point defects that are difficult to understand through experimental results alone. Here, we report the strong enhancement of the photoluminescence (PL) of $Y_2O_3:Bi^{3+}$ via codoping with Li^+ ions and suggest a plausible mechanism for that enhancement using both experimental and computational studies. The codoping of Li^+ ions into the $Y_2O_3:Bi^{3+}$ phosphor was found to cause significant changes in its structural and optical properties. Interestingly, unlike previous reports on Li^+ codoping with several other phosphors, we found that Li^+ ions preferentially occupy interstitial sites of the $Y_2O_3:Bi^{3+}$ phosphor. Computational insights based on density functional theory calculations also indicate that Li^+ is energetically more stable in the interstitial sites than in the substitutional sites. In addition, interstitially doped Li^+ was found to favor the vicinity of Bi^{3+} by an energy difference of 0.40 eV in comparison to isolated sites. The calculated DOS showed the formation of a shallow level directly above the unoccupied 6p orbital of Bi^{3+} as the result of interstitial Li^+ doping, which may be responsible for the enhanced PL. Although the crystallinity of the host materials increased with the addition of Li salts, the degree of increase was minimal when the Li^+ content was low (<1 mol %) where major PL enhancement was observed. Therefore, we reason that the enhanced PL mainly results from the shallow levels created by the interstitial Li^+.

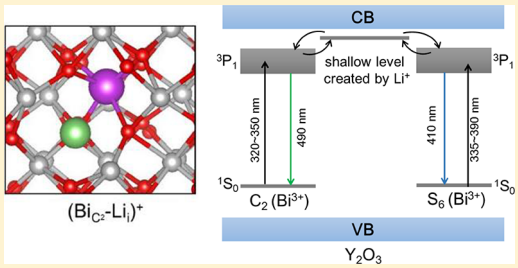

INTRODUCTION

An improved performance of displays and lighting requires high-quality phosphors with strong brightness and high stability.[1] To develop such phosphors, much attention has been paid to rare-earth activated metal oxide materials.[2] Among the metal oxide materials, yttrium oxide (Y_2O_3) has been widely studied as a host matrix for phosphors, since upon rare-earth doping (especially Eu^{3+}) it has proven to provide sufficient brightness for applications.[3,4]

Bismuth-doped yttrium oxide ($Y_2O_3:Bi^{3+}$) is one of the promising luminescent materials being developed for green/blue light emitting phosphors due to its chemical and physical stability and unique luminescent properties.[5] As represented in Figure 1, there are two different symmetries of Y sites in the Y_2O_3 crystal lattices, S_6 and C_2. The optical transitions $6s6p \rightarrow 6s^2$ of the doped Bi^{3+} in Y_2O_3 produce two broad photoluminescence (PL) peaks at 410 and 500 nm by excitations at around 378 and 325 nm, respectively, due to the two different symmetries. Owing to such properties of broadband absorption and emission, Bi-doped Y_2O_3 phosphor is considered as a potential material not only for light-emitting devices but also for third-generation photovoltaics.[5,6] In addition, Bi^{3+} ions are often codoped with rare-earth dopants to help enhance their PL intensity via energy transfer.[7,8] However, currently the luminescent intensity of the $Y_2O_3:Bi^{3+}$ phosphor is below satisfactory, and therefore there is much room left for improvement.

Jacobsohn et al. reported the synthesis of $Y_2O_3:Bi^{3+}$ phosphor by the combustion method and tried to improve its PL intensity by choosing different fuels, which enabled them to produce different temperatures during the combustion

Received: May 26, 2017
Published: September 29, 2017

DOI: 10.1021/acs.inorgchem.7b01353
Inorg. Chem. 2017, 56, 12139−12147

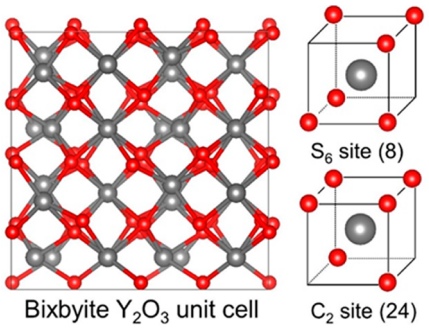

Figure 1. Atomic model of the bixbyite structure. Red spheres are oxygen atoms, and gray spheres are yttrium atoms. The values in parentheses are the numbers of sites in a unit cell.

process.[9] Huang et al. used postannealing to enhance the PL intensity of the Y_2O_3:Bi^{3+} phosphor.[7] Our laboratory also reported a method to increase the luminescence of the Y_2O_3:Bi^{3+} phosphor on the basis of a computational study.[10] In that investigation, we found that oxygen vacancies absorb the emissions from Bi and demonstrated that increasing the oxygen partial pressure during the annealing step of the Y_2O_3:Bi^{3+} phosphor to minimize the oxygen vacancies can help to enhance its PL intensity.

Recently, the presence of alkali ions (such as Li^+, Na^+, and K^+) was reported to enhance the luminescence of several oxide phosphors.[11−13] The alkali ions were previously suggested to produce a fluxing effect (the effect of the presence of molten salts: e.g., crystal growth, smoother surface, and stabilized phase),[14] a doping effect,[15] a charge imbalance/compensation,[12] or an effect through the removal of quenching centers (e.g., OH and NO_x).[16] The Li^+ ion, in particular, has been considered to affect the luminescence exclusively by doping. Being the smallest cation, it easily incorporates into a host matrix and thereby disturbs the local symmetry of the activator ions (e.g., lanthanide ions), which often results in an increase in luminescence. Singh et al. have reported the use of Li^+ ions to enhance the luminescence of lanthanide ions in several oxide phosphors and published a review in 2014 regarding the role of the Li^+ ion in phosphors.[13] That paper may be the first comprehensive review on Li doping in phosphors. The review provides several examples where Li^+ ions were used to enhance the luminescence of lanthanide ion doped Y_2O_3. However, the different research groups each suggested various mechanisms for the effect.

For example, Fan et al. studied the effects of Li^+ doping on Y_2O_3:Yb^{3+} nanocrystals and reported that doping with Li^+ enhanced their luminescence intensity by a factor of 12.[17] They explained that the enhancement could be mainly attributed to the modified local symmetry produced around the Yb^{3+} ions by codoping of Li^+. Shin et al., however, examined cathodoluminescence of the Li-doped Y_2O_3:Eu and suggested that the substitution of Y^{3+} ions by Li^+ ions might relieve the oxygen vacancies on the surface of the phosphor.[18] On the other hand, Yi et al. reported that the beneficial effects of the Li^+ ions on the Y_2O_3:Eu were mostly due to the improved crystallinity and reduced internal reflection by the rougher surface.[19] One of most recent examples is the work by Rai et al., where Li^+ ion doping to Bi^{3+}/Yb^{3+}-doped gadolinium tungstate was shown to enhance its quantum-cutting efficiency as much as 43%.[20] They believed that, in addition to the enhanced crystallinity of the phosphor by Li^+ ions (a flux effect), the charge imbalance and modified local crystal fields around Bi^{3+} and Yb^{3+} (a doping effect) are responsible for the enhancement.

Here we demonstrate the doping of Li^+ ions into the Y_2O_3:Bi^{3+} phosphor and a significant enhancement in its luminescence. To understand the mechanism of the enhancement, we used ab initio calculations and thermodynamics modeling. Our experimental results closely matched our theoretical predictions, and further we found the unexpected roles of interstitially doped Li^+ in blue and green light emission of Y_2O_3:Bi^{3+}.

EXPERIMENTAL AND COMPUTATIONAL SECTION

Synthesis. The solution combustion method was used for the synthesis of all the phosphors.[10] The nitrate precursors of Y^{3+} and Bi^{3+}, $Y(NO_3)_3{\cdot}6H_2O$ and $Bi(NO_3)_3{\cdot}6H_2O$, were purchased from Alfar Aesar, $Li(NO_3)$ salts were purchased from Daejung Chemical Co., and urea (NH_2CONH_2) was purchased from Junsei, Japan, and used as a fuel. The composition was selected as follows:

$$0.99[Y(NO_3)_3{\cdot}6H_2O] + 0.01[Bi(NO_3)_3{\cdot}6H_2O] + x[LiNO_3] + 2CH_4N_2O \rightarrow 1/2(Y_{0.99}Bi_{0.01})_2O_3 + x/2Li_2O + ((7 + x)/2)N_2 + 2CO_2 + nH_2O$$

where x = 0, 0.003, 0.005, 0.01, 0.03, 0.05. The Bi amount was fixed to 1% with respect to Y sites in the Y_2O_3 host because it was found to give an optimal green emission (see Figure S1 in the Supporting Information for PL intensities by different Bi doping amounts, 1, 3, and 5 mol %) and it is in good agreement with a previous report by Jacobsohn et al.[21] Lithium was added up to 5% to the total amount (1 mmol) of trivalent metal ions (Y^{3+} and Bi^{3+}).

$Y(NO_3)_3{\cdot}6H_2O$ (0.99 mmol), $Bi(NO_3)_3{\cdot}6H_2O$ (0.01 mmol), $Li(NO_3)$ (0.001−0.05 mmol), and urea (0.002 mol) were dissolved in deionized[14] water (50 mL). A homogeneous transparent solution was obtained after stirring vigorously for 20 min. The solution was placed into a preheated furnace at 500 °C in air. After all the liquid evaporated, a flame formed with a large amount of gases. The solid product was obtained in a foamy form, as it swelled to a larger volume due to the gaseous byproducts. The entire combustion process was completed within a few minutes. A subsequent heat treatment was conducted at 600 °C for 2 h under atmospheric conditions to remove any residual carbon and nitrogen impurities.

Instrumental Methods. Morphological observation and high-resolution transmission electron microscopy (HRTEM) images were obtained with a FEI Tecnai G2 instrument with an acceleration voltage of 300 kV. The crystal structure was studied by X-ray diffraction (XRD) (D8 Advanced, Bruker Corporation). Elemental analysis was performed with an inductively coupled plasma/mass spectrometer (ICP/MS) (ElAN DRC PLUS, PerkinElmer, US). Photoluminescence (PL) and decay time were determined with an ultrafast laser instrument (Spectra Physics, MaiTai HP). Each measurement was repeated three times, and an average value is provided in the text.

Computational Methods. Density functional theory (DFT) calculations were performed to calculate the doping energies of Li^+ and formation energies of defects in Y_2O_3:Bi^{3+}. We used the generalized gradient approximation (GGA) with Perdew−Burke−Ernzerhof (PBE) parametrization as implemented in the VASP software.[22,23] Atomic nuclei and core electrons were described by a projector-augmented wave (PAW).[24] Kohn−Sham orbitals were expanded with a cutoff energy of 400 eV, and a 3 × 3 × 3 equally spaced k-point grid was used for the Brillouin zone sampling.[25] In the defect formation energy calculations, the experimental binding energy of an oxygen molecule, 2.56 eV/atom, was employed instead of the GGA value to avoid overestimating the strength of the double bond (O═O) in the GGA calculations. The cell volume and all atoms were fully relaxed.

For the calculations of the formation energies of dopants and defects with charges, we employed the equation

DOI: 10.1021/acs.inorgchem.7b01353
Inorg. Chem. 2017, 56, 12139−12147

$$\Delta E^f(q) = E[D^q] \pm \mu_i - E^0 + q(E_v + \Delta V + \varepsilon_F) \quad (1)$$

where $E[D^q]$ is the total energy of the Y_2O_3 supercell with dopants or/and defects with a charge q, E^0 is the total energy of the defect-free Y_2O_3, μ_i is the chemical potential of the element i added to (removed from) the supercell to generate a point defect, E_v is the valence band maximum (VBM) of the defect-free Y_2O_3, ΔV is the shift of the VBM in the defective cell by a point defect relative to that in the defect-free Y_2O_3, and ε_F is the Fermi level referenced to E_v. The lattice constant and the formation energy of Y_2O_3 crystals obtained by the PBE method match well to the experimental values—error ratios were 0.001% and 0.9%, respectively (see our previous result in ref 10). Hence, we used the PBE method to calculate the formation energies of defects and dopants. PBE results are not presented much in our paper because those calculations were done to correct the results from PBE +U using eq 2 (this correction was inevitable since the system was too large to use higher-accuracy methods (e.g., HSE) with our limited computational resources). A Hubbard U approximation (U_{4d} = 6 eV) term[26] was included to correct the splitting of the 4d orbital of yttrium, and the spin−orbit coupling (SOC) was included for the correct description of the bismuth orbitals, as demonstrated in our recent work.[10] The Hubbard U, however, does not fully correct the band gap, the transition point of the defect charge. Hence, we extrapolated the transition point of the defect charge from PBE to PBE+U to obtain the exact value inexpensively using the equation[26,27]

$$\epsilon(q/q') = \epsilon(q/q')^{PBE+U} + \frac{\Delta\epsilon}{\Delta E}(E_g^{exp} - E_g^{PBE+U}) \quad (2)$$

with

$$\frac{\Delta\epsilon}{\Delta E} = \left(\frac{\epsilon(q/q')^{PBE+U} - \epsilon(q/q')^{PBE}}{E_g^{PBE+U} - E_g^{PBE}}\right) \quad (3)$$

where $\epsilon(q/q')$ is the transition point from charge q to q'. E_g^{exp},E_g^{PBE+U}, and E_g^{PBE} are the band gap energies obtained from experiments, PBE +U, and PBE, respectively. The coefficient $\Delta\epsilon/\Delta E_g$ is the rate of charge transition level change with respect to the change in band gap.

RESULTS AND DISCUSSION

Figure 2 shows the XRD patterns of the Y_2O_3 host and the xLi-doped $(Y_{0.99}Bi_{0.01})_2O_3$ phosphors (x = 0, 0.3, 0.5, 1, 3, 5 mol % with respect to Y^{3+}) prepared by the combustion method. The cubic phase of Y_2O_3 was observed in all compositions with no apparent impurity phases, and the diffraction peaks were well matched with JCPDS #82-2415 (cubic Y_2O_3) (see Figure S2 in the Supporting Information for XRD patterns up to 20% Li content). When the the Li^+ content was increased, the diffraction peak became narrower and the peak intensity grew distinctively higher, indicating the grain growth by the addition of Li(NO_3). The average crystallite sizes (Å, in diameter) of the phosphors with different Li fractions were calculated using the Debye−Scherrer equation[28] with full-width at half maximums (fwhms) of (222) planes and are shown in Table 1. The Li contents of 0.3 and 0.5 mol % did not provide much growth of the crystalline size of Y_2O_3, but those of 3 and 5 mol % showed a distinctive increase (almost twice) in the crystalline size.

To study the doping behavior of Li^+ ions in Y_2O_3:Bi^{3+} crystals in detail, slow-scanned XRD spectra were obtained with (222) planes and are shown in Figure 3. When 1 mol % of Bi^{3+} was introduced into the Y_2O_3 host lattice, the diffraction peak shifted to a higher angle, implying the contraction of cell volume (Figure 3b). Since the ionic radius of Bi^{3+} is similar to or slightly greater than that of Y^{3+},[7,29,30] the contraction might be due to the increased covalency by the Bi $6s^2$ lone-pair character.[31,32]

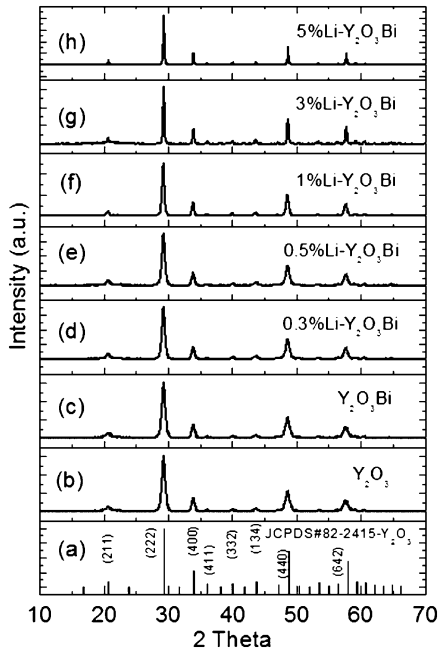

Figure 2. Powder XRD spectra of (a) Y_2O_3 and (b−h) $(Y_{0.99}Bi_{0.01})_2O_3/x$Li ($x$ = 0, 0.3, 0.5, 1, 3, 5 mol %).

Table 1. Crystal Information of Y_2O_3 and $(Y_{0.99}Bi_{0.01})_2O_3/x$Li ($x$ = 0, 0.3, 0.5, 1, 3, 5 mol %)

sample	fwhm (degree)	crystallite size (Å)
Y_2O_3	0.4985	154.2
Y_2O_3:Bi^{3+}	0.5563	143.0
Y_2O_3:Bi^{3+}/0.3%Li^+	0.5478	145.2
Y_2O_3:Bi^{3+}/0.5%Li^+	0.5583	142.4
Y_2O_3:Bi^{3+}/1%Li^+	0.4610	162.6
Y_2O_3:Bi^{3+}/3%Li^+	0.2642	302.3
Y_2O_3:Bi^{3+}/5%Li^+	0.2201	377.1

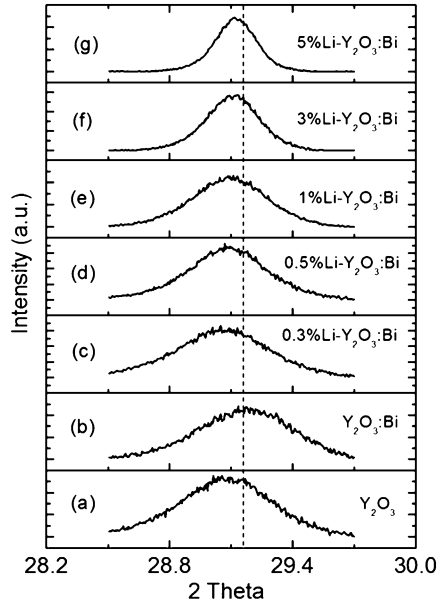

Figure 3. Slow-scanned XRD spectra of (a) Y_2O_3 and (b−g) $(Y_{0.99}Bi_{0.01})_2O_3/x$Li ($x$ = 0, 0.3, 0.5, 1, 3, 5 mol %) at the plane (222).

DOI: 10.1021/acs.inorgchem.7b01353
Inorg. Chem. 2017, 56, 12139−12147

On the other hand, when the phosphor was codoped with Li^+ content as little as 0.3 mol % (Figure 3c), the peak shifted significantly to a lower angle. However, when the Li contents were raised above 0.3 mol % (Figure 3c–g), the peak gradually shifted toward a higher angle than that with 0.3 mol % Li.

Considering the effective ionic radii of Li^+ and Y^{3+} (0.68 and 0.93 Å, respectively[12,33,34]), the Li^+ ion is small enough to enter any crystal site, such as Y^{3+} sites within the host lattice and interstitial sites. If the substitutional occupation by Li^+ is dominant, a lattice contraction will be found, whereas if the interstitial occupation is dominant, a lattice expansion will result.[12,33,34] Thus, the observed peak shift upon Li doping indicates that the interstitial doping preferentially occurs while substitutional doping partially contributes.

Due to its small size, Li has been considered by many researchers to dominantly occupy the Y^{3+} site, and the interstitial doping of Li^+ into the Y_2O_3 host was only suggested in the case of high Li content.[35,36] However, we observed that lattice expansion occurred with a Li^+ introduction of as little as 0.3 mol %, implying the dominant interstitial doping. Furthermore, when the Li content was raised above 0.3 mol %, slight lattice contraction occurred in comparison with the 0.3 mol % Li-doped phosphor. This observation suggests that in our Y_2O_3:Bi^{3+} phosphor the interstitial doping of Li is preferable to substitutional doping. Substitutional doping may occur in combination with the interstitial doping, especially under circumstances of Li contents higher than 1 mol %.

Unlike our results, when Mishra et al. observed Li ion doping in Y_2O_3:Er^{3+} nanophosphors, they reported that the diffraction peak (222) for Y_2O_3 shifts gradually toward a higher angle with Li contents up to 5 mol % and moves toward a smaller angle with a further increase in Li^+ content above 5 mol %.[16] Chung et al. also reported a similar trend with Li doping in a $CaMoO_4$ host.[37] As noted above, we not only observed the opposite trend in the peak shift but also found little change in peak shift above 5 mol % (see Figures S2 and S3 in the Supporting Information for XRD with higher Li content up to 20 mol %).

Intrigued by the XRD result, we raised a question of whether or not all the Li(NO_3) salts added during the combustion reaction were included in the host. Thus, we performed elemental analysis on the Li-doped Y_2O_3:Bi^{3+} phosphors after exclusive washing with water and compared the results with those obtained for the as-prepared samples (Table 2).

Table 2. Relative Elemental Compositions of As-Prepared and Water-Washed $(Y_{0.99}Bi_{0.01})_2O_3/xLi$ (x = 1, 5 mol %) by ICP

	elemental composition (mol %)		
sample	Y	Bi	Li
x = 1, as-prepared	98.58	0.79	0.63
x = 1, washed	98.66	0.83	0.51
x = 5, as-prepared	95.14	0.89	3.97
x = 5, washed	98.29	0.88	0.83

Interestingly, the sample with a Li content of 1 mol % showed similar Li contents for both the as-prepared and the water-washed cases (0.63 and 0.51 mol %, respectively), but the sample with an Li content of 5 mol % showed a large difference between the as-prepared and the water-washed cases (3.97 and 0.83 mol %, respectively). This result indicates that the doping concentration of Li is not heavily affected by the initial concentration of Li and there is a limit (<1 mol %) in the Li doping of the Y_2O_3:Bi^{3+} host, which explains the slight changes in the XRD peak shift by the amount of Li doping (0.3–5.0 mol %). This also shows that the excess Li salts may reside in the intergranular space rather than inside the Y_2O_3 host matrix, affecting the crystal growth of Y_2O_3.

To examine the morphological change produced by Li^+ addition, TEM analysis was conducted on the Y_2O_3:Bi^{3+} phosphors (Figure 4). Without Li doping a flat-sheet structure

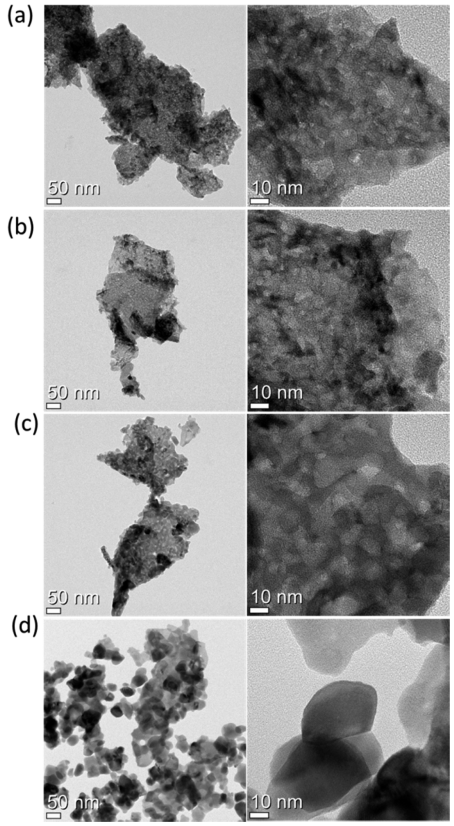

Figure 4. TEM images of $(Y_{0.99}Bi_{0.01})_2O_3/xLi^+$ of (a–d) x = 0, 0.5, 1, 5 mol %.

composed of highly aggregated small particles was observed. The combustion synthesis was conducted by the exothermic redox reactions of the precursor mixture (metal nitrates, oxidizers, and a fuel), and upon heating a spontaneous flame forms with a large amount of gases. Therefore, the solid product swells to a larger volume. Given the swelling and the fast formation time, it is not uncommon to obtain metastable materials with less-defined surface morphology.[21] With the introduction of Li ions of contents 0.5 and 1 mol %, flat-sheet structures were still observed but larger crystalline sizes were found. When the Li content was 5 mol %, the flat-sheet structure was disturbed and a highly crystalline particulate structure with an average size of less than 50 nm was formed, which is in good accordance with the XRD analysis. Along with the ICP results, these changes in particle morphology by the different Li contents strongly suggest that the Li reagent functions as a flux during the combustion reaction and its fluxing effect grows larger with its increasing amount.

Next, the effect of the Li^+ ions on the luminescent properties of Y_2O_3:Bi^{3+} was studied. The photoluminescence (PL) spectra of $(Y_{0.99}Bi_{0.01})_2O_3$ undoped and doped with Li up to 5 mol % are shown in Figure 5. A broad green emission at around 500

DOI: 10.1021/acs.inorgchem.7b01353
Inorg. Chem. 2017, 56, 12139–12147

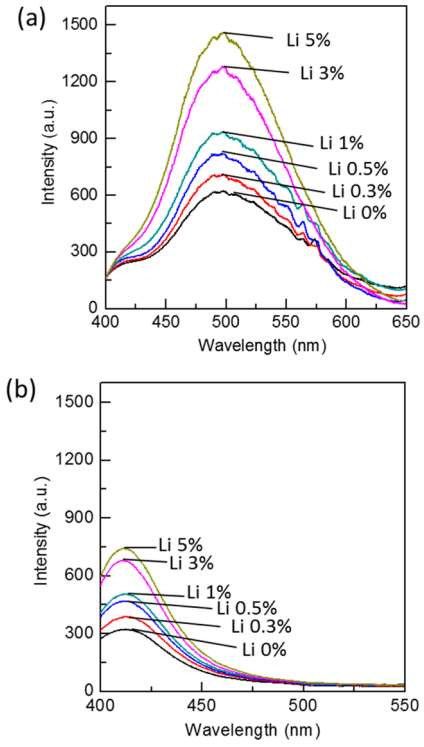

Figure 5. Luminescence properties of $(Y_{0.99}Bi_{0.01})_2O_3$ undoped and doped with Li up to 5 mol %: (a) C_2 PL emission spectra excited by 335 nm; (b) S_6 PL emission spectra excited by 378 nm.

nm was observed for the excitation at 335 nm, whereas a narrow blue emission at 410 nm was observed for the excitation at 378 nm. The two different emissions correspond to two different sites of Bi doping in the Y_2O_3 host: namely, C_2 and S_6 symmetry. The emission behavior of Y_2O_3:Bi^{3+} is due to the electronic transition of Bi^{3+}:$^3P_1 \rightarrow {}^1S_0$ in the Y_2O_3 host lattice.[6,21,38] Because of the different occupancies of the Bi^{3+}ions (see Figure 1, C_2(24) vs S_6(8)), the C_2 emission is more intense than the S_6 emission.[21]

The plots of relative PL enhancements as a function of Li contents for C_2 and S_6 emission showed two different slopes (Figure 6). One is an initial slope obtained from 0 to 0.5 mol %, and the other is a later slope obtained from 1 to 5 mol % of Li contents. The average initial slope of C_2 and S_6 emission is 0.74 (a = 0.609 for C_2 and a = 0.875 for S_6), while the later slope is 0.22 (a = 0.250 for C_2 and a = 0.183 for S_6). This trend in the PL enhancements by Li content indicates that the Li^+ ions play

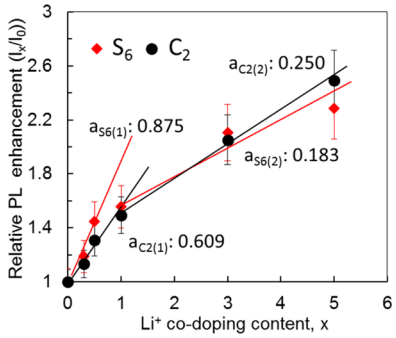

Figure 6. Relative PL enhancement of $(Y_{0.99}Bi_{0.01})_2O_3/xLi^+$ as a function of Li content (x, mol %).

multiple roles in the luminescence of the Y_2O_3:Bi^{3+} phosphor. At low Li^+ concentration (especially less than 1 mol %), the enhancement is mainly attributed to the Li doping to the host lattice. This notion is well supported by the ICP result (Table 2) for the phosphor with a Li content of 1 mol %, which showed that most of the Li^+ ions remained after exclusive washing with water. In addition, the significant increase in the PL intensity with Li contents of 0.3 and 0.5 mol % despite their similar crystallite sizes in comparison to Li-undoped phosphor (see Table 1 and Figure 4 for XRD and TEM) implies that the Li doping plays a major role in the enhancement. However, in a different phosphor ($KMg_4(PO_4)_3$:Eu^{2+}), multiple roles of Li^+ such as flux effect, crystal field splitting, and a reduction in concentration quenching were previously suggested by Liu et al.[11]

An Li content of above 1 mol % provided a further but slight increase in PL intensity. As proven by the XRD and TEM observations, a high content of Li^+ (especially above 1 mol %) drastically increases the crystallinity of the Y_2O_3:Bi^{3+} phosphor, indicating the flux effect of the $Li(NO_3)$ salt. The higher crystallinity results in higher oscillating strengths for the optical transition and fewer surface defects attributed to the PL increase.[19] When we plot the crystallite sizes and PL enhancements together, it appears clearer that the initial PL enhancement is due to the Li doping and the later enhancement is due to the increased crystallinity (Figure 7).

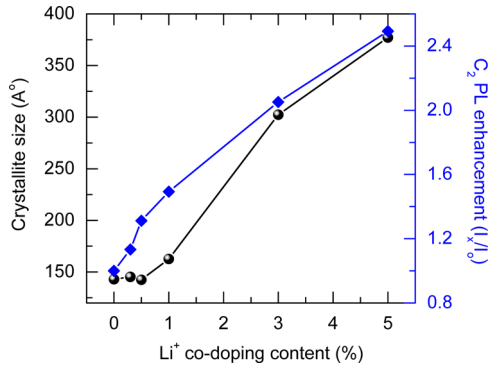

Figure 7. Relative PL enhancement vs crystallite sizes of $(Y_{0.99}Bi_{0.01})_2O_3/xLi^+$ as a function of Li content (x, mol %).

To further elucidate the mechanism of Li^+ ion doping in the Y_2O_3:Bi^{3+} phosphor, especially with respect to the low Li content, we conducted DFT thermodynamics calculations. For the calculation, a primitive unit cell of bixbyte Y_2O_3 crystal, which consists of 80 atoms (32 Y and 48 O atoms), was used. The cell size for Bi-doped Y_2O_3 was tested in our previous report[10] and compared to the 2 × 1 × 1 supercell, showing the negligible differences in the formation energies of oxygen vacancy defects and Bi doping (less than 0.03 eV/defect). Therefore, different configurations depending on the size of the supercell were not considered.

According to our previous results,[10] the Bi configuration was fixed to the substitutional site of the Y_2O_3 matrix, represented as Bi_{C2} and Bi_{S6} for the C_2 and S_6 sites of the Y_2O_3 matrix, respectively. The configuration for Li was tested for the substitutional and interstitial sites, represented as Li_Y^{2-} and Li_i^+, respectively. Configurations of Bi_{C2} and Bi_{S6} are net zero, since both Bi and Y are trivalent but Li_Y^{2-} and Li_i^+ are charged due to the difference in the charge states of Y sites (or interstitial sites)

DOI: 10.1021/acs.inorgchem.7b01353
Inorg. Chem. 2017, 56, 12139−12147

and Li^+. The equations used for the substitutional and interstitial lithium doping are

$$\frac{1}{2}Li_2O + Y_Y^x + O_O^x \rightarrow Li_Y^{2-} + V_O^{2+} + \frac{1}{2}Y_2O_3(s) \quad (4)$$

$$Li_2O \rightarrow 2Li_i^+ + O_i^{2-} \quad (5)$$

where V_O is an oxygen vacancy and O_i is an interstitial oxygen. The energetics of all possible reactions, including the formations of dopant−defect and dopant−dopant complexes with varying charge states, were considered (e.g., $(Bi_{C2}\text{-}Li_i)^+$, $(Bi_{S6}\text{-}Li_i)^+$, and $(Bi_Y\text{-}O_i)^{2-}$).

The calculated defect formation energies in Y_2O_3:Bi^{3+} with Li codoping at T = 1300 K under atmospheric pressure (P_{O2} = 0.21 atm) are shown in Figure 8. The formation energy

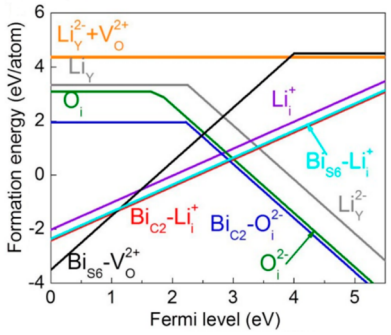

Figure 8. Calculated formation energies of Li^+ dopants, defects, and their complexes in bixbyite Y_2O_3.

($\Delta E^f(q)$) of Li_i^+ and O_i^{2-} (eq 5) was determined to be 0.26 eV, as driven by the cross point of the formation energy lines for $(Bi_{C2}\text{-}Li_i)^+$ (red line) and $(Bi_{C2}\text{-}O_i)^{2-}$ (blue line), keeping the charge balanced. The Fermi level satisfying the charge neutrality is 2.93 eV, where the concentrations of positive and negative defects/dopants are in balance. The concentrations of Li^+ and O_i^{2-} are determined by the Boltzmann factor

$$[D^q] = c_0 \exp\left[-\frac{\Delta E^f(q)}{k_B T}\right] \quad (6)$$

where c_0 is the concentration of available defect sites. However, since the magnitudes of charges of Li^+ and O_i^{2-} are different, the formation energy should be adjusted to satisfy charge balance conditions such that

$$[Li_i^+] = 2[O_i^{2-}] = c_0 \exp\left[-\frac{\Delta E_0^f + \Delta}{k_B T}\right] \quad (7)$$

ΔE_0^f is the formation energy at the crossing point between $(Bi_{C2}\text{-}Li_i)^+$ and $(Bi_{C2}\text{-}O_i)^{2-}$ in Figure 8. The magnitude of energy adjustment ($|\Delta|$) in the dilute case is estimated as $|\Delta| \leq k_B T \ln 2$, which is only 0.076 eV for the processing conditions (T = 1300 K). As the concentrations of Li_i^+ and O_i^{2-} are 6.92 × 10^{20} and 3.46 × 10^{20} cm^{-3}, respectively, when Δ is zero, the defect concentrations are on the order of 10^{20} cm^{-3}.

According to Figure 8, a doped Li^+ ion is energetically more stable in the octahedral interstitial sites (purple line: Li_i^+) rather than in the substitutional Y sites (gray line: Li_Y) of Y_2O_3. It is also found the interstitially doped Li favors the vicinities of Bi^{3+} at both C_2 and S_6 sites (red and cyan lines: $(Bi_{C2}\text{-}Li_i)^+$and $(Bi_{S6}\text{-}Li_i)^+$) by an energy difference of 0.40 and 0.34 eV, respectively, in comparison with isolated sites (purple line: Li_i^+). Subsequently, the probability of a solid solution of Li^+ in Bi^{3+}-doped Y_2O_3 was found to be about 15 times higher than that in pure Y_2O_3. To test this notion, we measured relative elemental compositions of Y_2O_3:Bi^{3+} with 15 mol % Li, changing the amounts of Bi addition from 0 to 5 mol % (Table 3). Given the findings in Table 2, we only examined the water-

Table 3. Relative Elemental Compositions of Water-Washed $(Y_{1-y}Bi_y)_2O_3$/15 mol % Li (y = 0, 0.01, 0.03, 0.05) by ICP

	elemental composition (mol %)		
$(Y_{1-y}Bi_y)_2O_3$ with 15 mol % Li	Y	Bi	Li
y = 0	99.81		0.19
y = 0.01	98.10	0.85	1.05
y = 0.03	91.63	3.47	4.90
y = 0.05	87.10	5.70	7.20

washed samples. The Li uptake significantly changed according to the Bi amount (it increased from 0.19 to 7.20 mol % as the Bi-doping amount was raised from 0 to 5.7 mol %), which is consistent with the theoretical suggestion. The observed Li contents were about 20−40% in excess of Bi contents (for 3 mol % Bi doping, ∼40% Li excess; for 5 mol % Bi doping, ∼26% Li excess). Although the calculated formation energies show that Li, when it is doped in the Y_2O_3:Bi crystal, is energetically more stable in the interstitial site, especially next to the Bi ions (represented as $Bi_{C2}\text{-}Li_i^+$ in Figure 8), than in the substitutional sites (represented as Li_Y in Figure 8), they do not imply that it is possible for only one interstitial Li to be present for each Bi dopant. The excess amount of Li is surmised to appear due to interstitially doped Li^+ that is unbound with Bi atoms (represented as Li_i^+ in Figure 8), since the formation energy difference of Li_i^+ and $Bi_{C2}\text{-}Li_i^+$ is only 0.3 eV. In addition, there must be unwashed Li^+ present on the surface of Y_2O_3 even after vigorous washing with water.

To compare our result to a reported system, we selected Er^{3+}-doped Y_2O_3 reported by Mishra et al.[16] and performed the DFT calculations on the system (see Figure S4 in the Supporting Information for calculated formation energies of Li^+ dopants in Er-doped Y_2O_3). Interestingly enough, we found that the formation energy of the interstitial lithium (Li_i^+) is considerably increased (+1.2 eV) near the Er^{3+} dopant of Y_2O_3:Er^{3+}, whereas that of the substitutional lithium (Li_Y^{2-}) is decreased (−0.2 eV) (the numbers are relative values in comparison to the formation energy of the lithium doped in pure Y_2O_3; a lower value means higher stability). The opposite trend was true with our Y_2O_3:Bi system—the relative formation energy for the interstitial lithium is −0.4 eV and that for the substitutional lithium is +0.2 eV, as shown in Table 4. This calculation suggests that the doping behavior of lithium is heavily influenced by other dopant ions.

To examine the effect of Li doping in the electronic structures of Y_2O_3:Bi^{3+}, electron densities of states (DOSs)

Table 4. Calculated Formation Energy Differences (eV) of Interstitial and Substitutional Lithiums in Y_2O_3:Er^{3+} vs Y_2O_3:Bi^{3+}

	Y_2O_3:Er	Y_2O_3:Bi
interstitial lithium (Li_i^+)	+1.2	−0.4
substitutional lithium (Li_Y^{2-})	−0.2	+0.2

DOI: 10.1021/acs.inorgchem.7b01353
Inorg. Chem. 2017, 56, 12139−12147

were calculated and are shown in Figure 9. The red line represents the DOS of the most stable atomic structure found

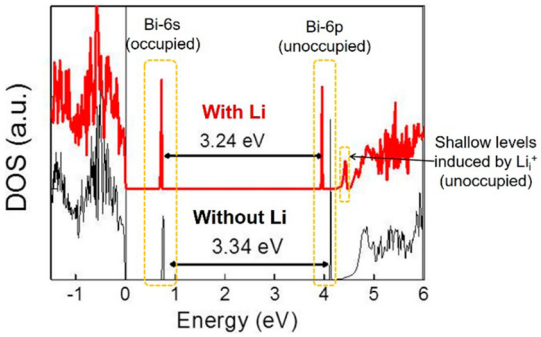

Figure 9. Calculated electron DOSs for Y_2O_3:Bi^{3+} with (red line) and without (black line) interstitially doped Li^+ ions. The energy level is with respect to the VBM.

in Figure 8, which is Y_2O_3:Bi^{3+} with interstitially doped Li^+ ions, and the black line represents that of Y_2O_3:Bi^{3+} without Li dopants. It is worth noting that shallow levels are formed right above the unoccupied 6p orbital of Bi only when Li_i^+ is codoped in Y_2O_3:Bi^{3+} (marked with an arrow). Such levels do not appear with the substitutional doping of Li^+ in Y_2O_3:Bi^{3+} (Figure S5 in the Supporting Information). When the atomic structures of Y_2O_3:Bi^{3+} phosphor with Li^+ ions at interstitial, S_6, and C_2 sites are graphically compared (Figure 10), it becomes

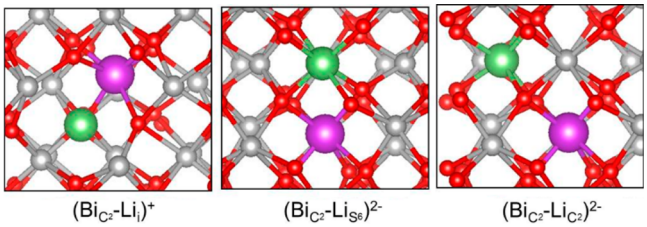

Figure 10. Calculated atomic structures of Bi^{3+} at C_2 sites and Li^+ ions at interstitial, S_6, and C_2 sites (from left to right) in the bixbyite Y_2O_3 matrix (the gray, purple, red, and green spheres are Y, Bi, O, and Li atoms, respectively).

clear that the interstitially doped Li ($(Bi_{C2}$-$Li_i)^+$) provides the shortest distance from the Bi atom, supporting our argument that the shallow level created by the interstitial Li is likely contributing to the Bi emission.

Since the interstitial Li^+ strongly favors locating in the vicinity of Bi^{3+} (Figure 8), we attribute the enhanced PL of Y_2O_3:Bi^{3+} by Li^+ to the hybridization of an Li_i^+-induced shallow level with the 6p orbital of Bi^{3+} near Li_i^+. It is worth noting that doping of Li^+ ions slightly alters the positions of the 6s and 6p orbitals of Bi^{3+} but does not create states between the 6s and 6p states of Bi. In our previous theoretical and experimental works, we showed that the oxygen vacancies create a deep unoccupied state in the middle of the Y_2O_3 band gap which reabsorbs green light from the Bi.[10] In contrast, Li^+ doping does not induce such in-gap states between the levels of the 6s and 6p orbitals of Bi^{3+}.

When shallow levels exist near the unoccupied orbital, two changes can be expected: (i) an increased lifetime of excitons due to shallow-level trapping and (ii) enhanced PL via charge transfer from the shallow level to the lower empty in-gap states. We therefore examined the exciton lifetime to verify our proposed model. Figure 11 shows representative PL decay curves of Y_2O_3:Bi^{3+} with 1 mol % Li (red line) and without

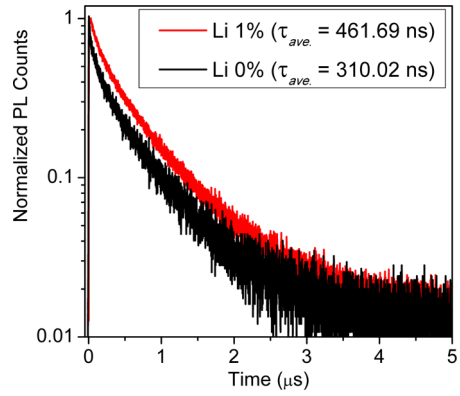

Figure 11. PL decay curves measured at the emission maximum (500 nm) for $(Y_{0.99}Bi_{0.01})_2O_3$ (black line) and $(Y_{0.99}Bi_{0.01})_2O_3$/1 mol % Li (red line).

(black line). Both decay curves fit very well with the third-order exponential function (eq 8):

$$Y_t = a_1 \exp(-t/\tau_1) + a_2 \exp(-t/\tau_2) + a_3 \exp(-t/\tau_3) + Y_0 \quad (8)$$

where Y_0 and Y_t are intensities at the initial state and at time t (ns), A is a constant, and τ is the decay time. The calculated average decay times were 310.02 and 461.69 ns for Y_2O_3:Bi^{3+} and 1 mol % Li doped Y_2O_3:Bi^{3+}, respectively. The increased lifetime was considered to result from the shallow levels created by the interstitially doped Li ions. The proposed mechanism of charge transfer in Y_2O_3:Bi^{3+} codoped with Li^+ ions is shown in Figure 12 (the gray, purple, red, and green spheres are Y, Bi, O,

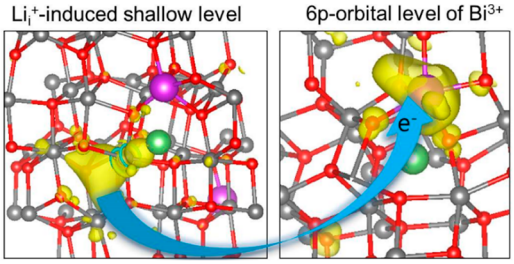

Figure 12. Charge transfer mechanism from the unoccupied Li_i^+-induced shallow level near the CBM of Y_2O_3 (left panel) to the Bi 6p orbital level (right panel). The gray, purple, red, and green spheres are Y, Bi, O, and Li atoms, respectively.

and Li atoms, respectively). The figure is drawn by the calculated local density of states, the sum of wave function norms for a given energy range, and shows the charge transfer from the unoccupied shallow level induced by Li_i^+ (left panel) to the Bi 6p orbital levels (right panel). The wave functions are highly localized at the Y sites induced by the interstitially doped Li^+ in the vicinity, and the unoccupied Bi 6p orbital is well-hybridized with the coordinate O 2p orbital (see the yellow isosurfaces on the O atoms in the right panel; one of the oxygen atoms links the Y atom with shallow level states and the doped Bi atom).

DOI: 10.1021/acs.inorgchem.7b01353
Inorg. Chem. 2017, 56, 12139−12147

CONCLUSION

Metal ion doped Y_2O_3 is of great interest as a luminescent material, since it is used commercially as a red-emitting phosphor. However, no clear understanding of its defect chemistry by doping has ever been provided. In this study, we initiated Li^+ codoping of the Y_2O_3:Bi^{3+} phosphor and thoroughly examined the structural and optical changes induced by Li^+. We found that the enhancement produced by a Li^+ concentration of over 1 mol % was mainly due to the flux effect of Li salts, while enhancement from a low Li concentration (<1 mol %) could be ascribed to the doping effect of Li^+. Using ab initio calculations and thermodynamic modeling, we discovered the doping nature of Li^+ in Y_2O_3:Bi^{3+}—Li^+ is energetically favorable in interstitial sites rather than in substitutional sites. We also found that interstitial Li^+ is more stable near Bi^{3+} dopants and contributes to charge transfers to the unoccupied 6p orbital of Bi^{3+} through the formation of a shallow level directly above it.

Our results indicate an important proof of concept regarding how calculations can be used to understand the defect chemistry of metal ion doped lanthanide oxide and improve its photoluminescence.

ASSOCIATED CONTENT

Supporting Information

The Supporting Information is available free of charge on the ACS Publications website at DOI: 10.1021/acs.inorgchem.7b01353.

PL intensities from different amounts of Bi doping (1, 3, and 5 mol %), XRD spectra of Li contents up to 20 mol %, calculated formation energies of Li^+ in Er-doped Y_2O_3 and Bi-doped Y_2O_3, and calculated electron DOSs for the substitutional doping of Li^+ in Y_2O_3:Bi^{3+} (PDF)

AUTHOR INFORMATION

Corresponding Author

*E-mail for S.-H.C.: sohyec@kist.re.kr.

ORCID

So-Hye Cho: 0000-0001-9707-8629

Author Contributions

⊥S.K. and H.C. contributed equally in this work.

Notes

The authors declare no competing financial interest.

ACKNOWLEDGMENTS

This work was supported by the institutional funding of the Korea Institute of Science and Technology (Grant No. 2E26960 and 2E26130) and the South Africa/South Korea joint collaboration program managed by the National Research Foundation (Grant No. SKOR15081792426/2014K1A3A1A09063246).

REFERENCES

(1) Nalwa, H. S.; Rohwer, L. S. *Handbook of luminescence, display materials, and devices*; American Scientific Publishers: Stevenson Ranch, CA, 2003.

(2) Wang, X. C.; Zhao, Z. Y.; Wu, Q. S.; Li, Y. Y.; Wang, Y. H. A Garnet-Based $Ca_2YZr_2Al_3O_{12}$:Eu^{3+} Red-Emitting Phosphor for n-UV Light Emitting Diodes and Field Emission Displays: Electronic Structure and Luminescence Properties. *Inorg. Chem.* **2016**, *55*, 11072−11077.

(3) Mishra, K. C.; Berkowitz, J. K.; Johnson, K. H.; Schmidt, P. C. Electronic-Structure and Optical-Properties of Europium-Activated Yttrium-Oxide Phosphor. *Phys. Rev. B: Condens. Matter Mater. Phys.* **1992**, *45*, 10902−10906.

(4) Devaraju, M. K.; Yin, S.; Sato, T. Eu^{3+}:Y_2O_3 Microspheres and Microcubes: A Supercritical Synthesis and Characterization. *Inorg. Chem.* **2011**, *50*, 4698−4704.

(5) Boulon, G. Photoluminescence Processes in Bi^{3+} Activated Polycristallines Rare-Earth Oxydes and Orthovanadates. *J. Phys. (Paris)* **1971**, *32*, 333−347.

(6) Schamps, J.; Flament, J. P.; Real, F.; Noiret, I. Ab initio simulation of photolumineseence: Bi^{3+} in Y_2O_3 (S-6 site). *Opt. Mater.* **2003**, *24*, 221−230.

(7) Huang, X. Y.; Ji, X. H.; Zhang, Q. Y. Broadband Downconversion of Ultraviolet Light to Near-Infrared Emission in Bi^{3+}−Yb^{3+}-Codoped Y_2O_3 Phosphors. *J. Am. Ceram. Soc.* **2011**, *94*, 833−837.

(8) Qu, M.; Wang, R.; Chen, Y.; Zhang, Y.; Li, K.; Yan, H. Broadband near infrared quantum cutting in Bi−Yb codoped Y_2O_3 transparent films on crystalline silicon. *J. Lumin.* **2012**, *132*, 1285−1289.

(9) Jacobsohn, L. G.; Tappan, B. C.; Tornga, S. C.; Blair, M. W.; Luther, E. P.; Mason, B. A.; Bennett, B. L.; Muenchausen, R. E. The effect of hydrostatic pressure on the combustion synthesis of Y_2O_3:Bi nanophosphor. *Opt. Mater.* **2010**, *32*, 652−656.

(10) Choi, H.; Cho, S. H.; Khan, S.; Lee, K.-R.; Kim, S. Roles of an oxygen Frenkel pair in the photoluminescence of Bi^{3+}-doped Y_2O_3: computational predictions and experimental verifications. *J. Mater. Chem. C* **2014**, *2*, 6017−6024.

(11) Chen, J.; Li, C. H.; Hui, Z.; Liu, Y. G. Mechanisms of Li^+ Ions in the Emission Enhancement of $KMg_4(PO_4)_3$:Eu^{2+} for White Light Emitting Diodes. *Inorg. Chem.* **2017**, *56*, 1144−1151.

(12) Shi, S.; Gao, J.; Zhou, J. Effects of charge compensation on the luminescence behavior of Eu^{3+} activated $CaWO_4$ phosphor. *Opt. Mater.* **2008**, *30*, 1616−1620.

(13) Singh, A. K.; Singh, S. K.; Rai, S. B. Role of Li^+ ion in the luminescence enhancement of lanthanide ions: favorable modifications in host matrices. *RSC Adv.* **2014**, *4*, 27039−27061.

(14) Ding, Y. J.; Yang, W. M.; Zhang, Q. T.; Wang, L. X. Influence of alkali metal compound fluxes on Gd_2O_2S:Tb particle and luminescence. *J. Mater. Sci.: Mater. Electron.* **2015**, *26*, 1982−1986.

(15) Fan, T.; Zhang, Q. Y.; Jiang, Z. H. Enhancement of the 1.5 μm emission in Y_2O_3:Er^{3+} nanocrystals by codoping with Li^+ ions. *J. Opt.* **2011**, *13*, 015001−015004.

(16) Mishra, K.; Singh, S. K.; Singh, A. K.; Rai, S. B. Frequency upconversion in Er^{3+} doped Y_2O_3 nanophosphor: Yb^{3+} sensitization and tailoring effect of Li^+ ion. *Mater. Res. Bull.* **2013**, *48*, 4307−4313.

(17) Fan, T.; Zhang, Q. Y.; Jiang, Z. H. Enhanced near-infrared luminescence in Y_2O_3:Yb nanocrystals by codoping with Li^+ ion. *Opt. Commun.* **2011**, *284*, 249−251.

(18) Shin, S. H.; Kang, J. H.; Jeon, D. Y.; Zang, D. S. Enhancement of cathodoluminescence intensities of Y_2O_3:Eu and Gd_2O_3:Eu phosphors by incorporation of Li ions. *J. Lumin.* **2005**, *114*, 275−280.

(19) Yi, S. S.; Bae, J. S.; Moon, B. K.; Jeong, J. H.; Park, J. C.; Kim, I. W. Enhanced luminescence of pulsed-laser-deposited Y_2O_3:Eu^{3+} thin-film phosphors by Li doping. *Appl. Phys. Lett.* **2002**, *81*, 3344−3346.

(20) Yadav, R. V.; Yadav, R. S.; Bahadur, A.; Singh, A. K.; Rai, S. B. Enhanced Quantum Cutting via Li^+ Doping from a Bi^{3+}/Yb^{3+}-Codoped Gadolinium Tungstate Phosphor. *Inorg. Chem.* **2016**, *55*, 10928−10935.

(21) Jacobsohn, L. G.; Blair, M. W.; Tornga, S. C.; Brown, L. O.; Bennett, B. L.; Muenchausen, R. E. Y_2O_3:Bi nanophosphor: Solution combustion synthesis, structure, and luminescence. *J. Appl. Phys.* **2008**, *104*, 124303−124307.

(22) Perdew, J. P.; Burke, K.; Ernzerhof, M. Generalized Gradient Approximation Made Simple. *Phys. Rev. Lett.* **1996**, *77*, 3865−3868.

(23) Perdew, J. P.; Burke, K.; Ernzerhof, M. Generalized Gradient Approximation Made Simple [Phys. Rev. Lett. 77, 3865 (1996)]. *Phys. Rev. Lett.* **1997**, *78*, 1396−1396.

DOI: 10.1021/acs.inorgchem.7b01353
Inorg. Chem. 2017, 56, 12139−12147

(24) Kresse, G.; Joubert, D. From ultrasoft pseudopotentials to the projector augmented-wave method. *Phys. Rev. B: Condens. Matter Mater. Phys.* **1999**, *59*, 1758−1775.
(25) Monkhorst, H. J.; Pack, J. D. Special points for Brillouin-zone integrations. *Phys. Rev. B* **1976**, *13*, 5188−5192.
(26) Freysoldt, C.; Grabowski, B.; Hickel, T.; Neugebauer, J.; Kresse, G.; Janotti, A.; Van de Walle, C. G. First-principles calculations for point defects in solids. *Rev. Mod. Phys.* **2014**, *86*, 253−305.
(27) Janotti, A.; Van de Walle, C. G. Native point defects in ZnO. *Phys. Rev. B: Condens. Matter Mater. Phys.* **2007**, *76*, 165202.
(28) Cullity, B. D.; Stock, S. R. *Elements of x-ray diffraction*, 3rd ed.; Prentice Hall: Upper Saddle River, NJ, 2001.
(29) Datta, R. Luminescent behavior of bismuth in rare-earth oxides. *J. Electrochem. Soc.* **1967**, *114*, 1137−1142.
(30) Bhavani, G.; Ganesan, S. Structural, morphological and optical study of bismuth and zinc co-doped yttrium oxide prepared by solvothermal and wet chemical method. *Acta Phys. Pol., A* **2016**, *130*, 1373−1379.
(31) Wolfe, R.; Newnham, R. Rare earth bismuth titanates. *J. Electrochem. Soc.* **1969**, *116*, 832−835.
(32) Shannon, R. D. Revised effective ionic radii and systematic studies of interatomic distances in halides and chalcogenides. *Acta Crystallogr., Sect. A: Cryst. Phys., Diffr., Theor. Gen. Crystallogr.* **1976**, *32*, 751−767.
(33) Dhananjaya, N.; Nagabhushana, H.; Nagabhushana, B. M.; Rudraswamy, B.; Shivakumara, C.; Narahari, K.; Chakradhar, R. P. S. Enhanced photoluminescence of Gd_2O_3:Eu^{3+} nanophosphors with alkali (M = Li^+, Na^+, K^+) metal ion co-doping. *Spectrochim. Acta, Part A* **2012**, *86*, 8−14.
(34) Bae, J.-S.; Hong, T.; Yoon, J.; Lee, B.; Won, M.-S.; Kim, J.; Kim, Y.; Jeong, J. Optical properties and surface analysis of lithium incorporated Y_2O_3:Eu^{3+} ceramic phosphors. *J. Anal. Sci. Technol.* **2010**, *1*, 92−97.
(35) Cheng, Q.; Sui, J. H.; Cai, W. Enhanced upconversion emission in Yb^{3+} and Er^{3+} codoped $NaGdF_4$ nanocrystals by introducing Li^+ ions. *Nanoscale* **2012**, *4*, 779−784.
(36) Yadav, R. V.; Singh, S. K.; Rai, S. B. Effect of the Li^+ ion on the multimodal emission of a lanthanide doped phosphor. *RSC Adv.* **2015**, *5*, 26321−26327.
(37) Chung, J. H.; Ryu, J. H.; Eun, J. W.; Lee, J. H.; Lee, S. Y.; Heo, T. H.; Shim, K. B. High enhancement of green upconversion luminescence of Li^+/Er^{3+}/Yb^{3+} tri-doped $CaMoO_4$. *Mater. Chem. Phys.* **2012**, *134*, 695−699.
(38) Vandecraats, A. M.; Blasse, G. The Quenching of Bismuth(III) Luminescence in Yttrium-Oxide (Y_2O_3). *Chem. Phys. Lett.* **1995**, *243*, 559−563.

DOI: 10.1021/acs.inorgchem.7b01353
Inorg. Chem. 2017, 56, 12139−12147